© 2018. Published by The Company of Biologists Ltd | Journal of Experimental Biology (2018) 221, jeb179085. doi:10.1242/jeb.179085

RESEARCH ARTICLE

Non-linear amplification of graded voltage signals in the first-order visual interneurons of the butterfly *Papilio xuthus*

Juha Rusanen[1], Roman Frolov[1,*], Matti Weckström[1], Michiyo Kinoshita[2] and Kentaro Arikawa[2]

ABSTRACT

Lamina monopolar cells (LMCs) are the first-order visual interneurons of insects and crustacea, primarily involved in achromatic vision. Here, we investigated morphological and electrophysiological properties of LMCs in the butterfly *Papilio xuthus*. Using intracellular recording coupled with dye injection, we found two types of LMCs. Cells with roundish terminals near the distal surface of the medulla demonstrating no or small depolarizing spikes were classified as L1/2. Cells with elongated terminals deep in the medulla that showed prominent spiking were classified as L3/4. The majority of LMCs of both types had broad spectral sensitivities, peaking between 480 and 570 nm. Depending on the experimental conditions, spikes varied from small to action potential-like events, with their amplitudes and rates decreasing as stimulus brightness increased. When the eye was stimulated with naturalistic contrast-modulated time series, spikes were reliably triggered by high-contrast components of the stimulus. Spike-triggered average functions showed that spikes emphasize rapid membrane depolarizations. Our results suggest that spikes are mediated by voltage-activated Na^+ channels, which are mainly inactivated at rest. Strong local minima in the coherence functions of spiking LMCs indicate that the depolarizing conductance contributes to the amplification of graded responses even when detectable spikes are not evoked. We propose that the information transfer strategies of spiking LMCs change with light intensity. In dim light, both graded voltage signals and large spikes are used together without mutual interference, as a result of separate transmission bandwidths. In bright light, signals are non-linearly amplified by the depolarizing conductance in the absence of detectable spikes.

KEY WORDS: Lamina monopolar cells, Insect vision, Japanese yellow swallowtail, Spectral sensitivity, Information processing

INTRODUCTION

In insects, the information gathered by photoreceptors in the compound eyes is processed in three successive visual neuropils: the lamina, the medulla and the lobula. The retina is composed of segregated units, ommatidia, each containing several photoreceptors of at least two spectral classes. In flies, the first visual interneurons in the lamina, lamina monopolar cells (LMCs), form synapses with six broadband-sensitive photoreceptors (R1–R6). These photoreceptors are called short visual fibers (SVFs). In contrast to photoreceptors, which respond to light stimulation with membrane depolarization, LMCs are sign-inverting neurons that utilize hyperpolarizing Cl^- current to process and transfer visual information. LMCs send their axons to the next visual neuropil (medulla), where they provide input to the motion-detection system (Joesch et al., 2010; Silies et al., 2013). Axons of other photoreceptors (usually R7 and R8) bypass the lamina and terminate directly in the medulla, and are therefore called long visual fibers (LVFs). Thus the SVFs and LMCs are thought to be specialized in achromatic vision, whereas the LVFs and medullar interneurons they connect to are mainly responsible for color vision (Heisenberg and Buchner, 1977; Yamaguchi et al., 2008).

Similar to photoreceptors in the retina, which modify their functions extensively as light intensity changes, LMCs adapt to different illumination conditions, low-pass filtering in dim light and band-pass filtering in bright light (van Hateren, 1992). Most of the mechanisms contributing to LMC responses and adaptation are thought to reside at the presynaptic photoreceptor side (reviewed by Laughlin, 2010). However, there is growing evidence that post-synaptic processes are also important (Laughlin and Osorio, 1989; Skingsley et al., 1995; Uusitalo et al., 1995; Rusanen and Weckström, 2016).

Although LMCs are traditionally regarded as graded potential-signaling neurons, it has been repeatedly shown that fast transient depolarizing events called spikes can be elicited (Järvilehto and Zettler, 1971; Zettler and Järvilehto, 1971; Hardie and Weckström, 1990; Rusanen et al., 2017). In the blowfly, spikes can be observed when a LMC is depolarized after light-induced hyperpolarization. Large spikes often resemble action potentials and thus are most likely mediated by voltage-gated Na^+ channels (Uusitalo et al., 1995). While spikes appear to contribute to amplification of high-frequency signals, the question about the role spikes play in information coding by LMCs remains unanswered (Uusitalo et al., 1995).

In this study, we performed intracellular recordings from LMCs of the butterfly *Papilio xuthus*, a highly visual diurnal insect species. Butterflies are characterized by a much greater diversity of spectral receptor types than any other insects described so far (Wakakuwa et al., 2007). *Papilio xuthus* possesses photoreceptors of six spectral classes, including ultraviolet, violet, blue, green, red and broad-band ones (Arikawa, 2003). These photoreceptors form ommatidia of three spectrally distinct types. Each ommatidium contains nine photoreceptor cells (R1–R9), including two green-sensitive R3 and R4 photoreceptors, and a variable set of other photoreceptors. Different types of ommatidia are randomly distributed throughout the retina. The R1 and R2 photoreceptors, which are ultraviolet, violet or blue sensitive, are the LVFs that terminate in the medulla, whereas green, red and broadband photoreceptors (R3–R8) are the SVFs that terminate in the lamina (Takemura et al., 2005). Although LVFs do not terminate in the

[1]Nano and Molecular Materials Research Unit, Faculty of Science, University of Oulu, PO Box 3000, Oulu 90014, Finland. [2]Laboratory of Neuroethology, Sokendai (The Graduate University for Advanced Studies), Hayama, Kanagawa 240-0193, Japan.

*Author for correspondence (rvfrolov@gmail.com)

R.F., 0000-0002-7431-5297

Received 7 February 2018; Accepted 26 April 2018

lamina, they make synaptic contacts with LMCs there (Takemura and Arikawa, 2006).

We investigated morphological and electrophysiological properties of LMCs in the butterfly, including spectral sensitivities. We describe two functional classes of LMCs – spiking and non-spiking ones – and propose that presumptive voltage-activated Na^+ (Na_V) channels non-linearly amplify stimulus intensity decrements by generating spikes in dim backgrounds, and increasing depolarizing transients in bright light.

MATERIALS AND METHODS

Animals

We used both sexes of the Japanese yellow swallowtail butterfly, *Papilio xuthus* Linnaeus 1767, which were derived from eggs laid by females collected in the field around Sokendai, Kanagawa, Japan. The hatched larvae were reared on fresh citrus leaves under a light regime of 10 h light:14 h dark, which induced pupal diapause. The pupae in diapause were stored at 4°C for at least 3 months, and were allowed to emerge at 20°C.

Preparation and intracellular recordings

Recording electrodes were pulled from quartz glass capillaries (1 mm o.d., 0.6 mm i.d., Sutter Instruments, Novato, CA, USA) with a laser puller (Model P-2000, Sutter Instruments), and filled with 2 mol l^{-1} potassium acetate buffered to pH 6.8 with KH_2PO_4. Electrode resistance was 180–220 MΩ. A small hole was made in the dorsal cornea of the left compound eye and covered with paraffin-based grease, through which a recording electrode was inserted into the retina and advanced further across the basement membrane until it reached the lamina. Recordings were performed in the lamina, from the somata of LMCs or from the synaptic zone. However, it cannot be excluded that some of the recordings were made from axons in the first optic chiasma. Successful LMC impalements were identified by resting potentials lower than −30 mV and hyperpolarizing responses to light. The reference electrode was inserted into the retina of the other eye. All experiments were performed at room temperature (20–22°C).

Staining and microscopy

The electrode tip was filled with 3% Neurobiotin™ tracer (Vector Laboratories, Burlingame, CA, USA) in 2 mol l^{-1} potassium acetate solution, and the rest of the electrode was filled with 2 mol l^{-1} potassium acetate solution (resistance 180–220 MΩ). After completion of electrophysiological measurements, the tracer was injected into the cell for 15–20 min, or until the cell was lost, by continuously applying 300 ms current pulses of 0.15–0.30 nA amplitude with 1 Hz frequency. Neurons were visualized as described previously (Hamanaka et al., 2013). The isolated eye, with the optic lobe and cornea still attached, was dissected and fixed overnight at 4°C in solution containing 4% paraformaldehyde, 0.25% glutaraldehyde and 0.2% picric acid in 0.1 mol l^{-1} phosphate buffer (PB, pH 7.4). Subsequently, the corneas were removed, the tissue was embedded in gelatin/albumin mixture and post-fixed overnight in 7.5% paraformaldehyde at 4°C. Next, the tissue was cut into 40 µm slices with a vibrating microtome (VT1000S, Leica Biosystems, Wetzlar, Germany). The slices were washed and then incubated in PB saline supplemented with streptavidin–horseradish peroxidase (0.5% RPN1051, Amersham Biosciences, Little Chalfont, UK) and 0.5% Triton X-100 (Sigma-Aldrich, St Louis, MO, USA) overnight at room temperature. The washed slices were developed with 0.03% 3,3′-diaminobenzidine tetrahydrochloride in 0.05 mol l^{-1} Tris-HCl (pH 7.4) containing 0.015% H_2O_2 and 0.3% nickel ammonium sulfate. After washing with PB, the slices were set on the gelatin-coated slide glass, dehydrated in an ethanol series, cleared in xylene and mounted in Entellan® (Merck Millipore, Billerica, MA, USA) under a coverslip.

Light stimulation

For light stimulation, 14 narrow-band light-emitting diodes (LEDs) with peak wavelengths of 355, 385, 400, 435, 450, 462, 490, 505, 525, 545, 572, 594, 612 and 625 nm were used. The light was led into the Faraday cage using a quartz light guide, the end of which was attached to the cardan arm rotation system. The angular size of the light source was ca. 6–7 deg. The maximal intensity of the 525 nm LED at the corneal surface was 14.6×10^{14} photons cm^{-2} s^{-1}. Other light intensities used in this work are expressed in log units relative to this intensity. LED brightness was controlled using a custom-made voltage-to-current converter and a set of neutral density (ND) filters, allowing control of stimulus intensity over 6 orders of magnitude. LED calibration was performed using a spectrometer (USB4000, Ocean Optics, Dunedin, FL, USA). Spectral sensitivities of LMCs were determined using a modified flash method as described previously (Rusanen et al., 2017). The isoquantal flash response series were usually recorded at least twice and the response amplitudes were averaged to improve accuracy.

To investigate the frequency responses of LMCs, we used two different (15 s) natural light intensity sequences (naturalistic stimuli, NS) from the van Hateren database (van Hateren, 1997). The NS were used to drive the 525 nm LED at four background intensities in conjunction with three ND filters, ND1–ND3, corresponding to $\log(I/I_0)$ values of −1, −2 and −3, where I_0 is the intensity of a non-attenuated stimulus; in the text and figures, the abbreviation ND0 is used to denote the brightest light level used. At each light intensity, the stimulation was repeated 5 times. LMC voltage responses were recorded at a sampling frequency of 2.4 kHz.

Data analysis

MatLab (R2015b) was used for data analysis. The transfer function $H(f)$ between NS (light stimulus input) and the LMC voltage response (output) was calculated as $H(f)=P_{xy}(f)/P_{xx}(f)$, where $P_{xx}(f)$ is the power spectrum density of the input and $P_{xy}(f)$ is the cross-power spectrum density of the input and output. Coherence between the input and output was calculated as $C(f)=|P_{xy}(f)|^2/[P_{xx}(f)P_{yy}(f)]$. To improve the accuracy of transfer function estimates, NS stimulation was repeated 5 times, with the first response omitted to ensure that the animal adapted to a new light level and the remaining four averaged. Power spectra were calculated using Welch's method with a 3 s Hamming window and a 50% overlap. The resulting transfer functions were smoothed using a 45-point median filter.

Many LMCs responded to NS with a combination of graded potentials and spikes. To examine the functional relationship between the aspects of the stimulus and spikes, we calculated the spike-triggered average (STA) as described previously (Rusanen et al., 2017), by excising and averaging stimulus segments preceding the spike. To detect a spike, an algorithm combining template matching with simple voltage thresholding was used. Spike templates were made on the basis of easily recognizable spikes characterized by fast transient kinetics and an amplitude of more than 10 mV, and were selected by visual inspection of voltage traces: 146 such spikes were selected from three LMCs at four light levels (ND0–3); of these, 97 spikes were randomly chosen and used for unsupervised clustering. Two distinct clusters were discovered

Journal of Experimental Biology (2018) 221, jeb179085. doi:10.1242/jeb.179085

and used to establish two spike templates by averaging the spikes in each cluster. The first template had an amplitude of 16.4±4.6 mV and a half-width of 3.6±0.7 ms (mean±s.d., n=22). The second template had an amplitude of 22.7±7.5 mV and a half-width of 3.6±0.9 ms (n=75). These templates were then used to detect spikes (Rusanen et al., 2017). The minimal spike amplitude was determined as mean minus 2 s.d. for the first template amplitude, 16.4−2×4.6=7.2 mV; the maximal spike half-width was determined as mean plus 2 s.d., 3.6+2×0.9=5.4 ms.

Statistics

Statistical group comparisons were performed in the following way. First, the Shapiro–Wilk normality test was applied to data samples to determine whether they could be analyzed using parametric statistical methods. As all our experimental groups passed the normality test, the data are presented as means±s.d. unless specified otherwise, and compared using a two-tailed unpaired t-test with unequal variances as indicated.

RESULTS

The experiments and analyses are divided into six sections. The first two sections address the general properties of butterfly LMCs, while the remaining sections are dedicated to functional electrophysiological analysis. Specifically, section 1 (see 'Morphology', below) describes the morphology and localization of LMC axons and terminals in the medulla (Fig. 1) and offers tentative classification of LMCs. Section 2 (see 'Spectral sensitivity', below) compares spectral sensitivity functions of photoreceptors and LMCs (Fig. 2). Sections 3–6 correspondingly describe: basic light responses ('Light responses', Figs 3 and 4); spiking ('Analysis of spiking properties', Figs 5–7); and the role of spikes in information processing ('Spikes and naturalistic stimulation' and 'Transfer functions'; Figs 8–10).

Morphology

Four different types of LMCs (L1–L4) have been previously identified in the Australian Orchard butterfly, *Papilio aegeus* (Ribi, 1987). In brief, L1 and L2 are characterized by dense dendritic processes throughout the depth of the lamina. L1 terminates in the medulla layer 1, and L2 in layer 2. L3 has sparse dendritic processes throughout the depth of the lamina, whereas L4 has processes only in the proximal region of the lamina. L3 and L4 terminate in layer 3 of the medulla. Similarly, four LMC types have been proposed for *P. xuthus* (Hamanaka et al., 2013), but the types of medulla terminals have not been correlated to the processes in the lamina. In this work, we followed the LMC classification procedure of Ribi (1987).

Based on the microscopic examinations of neurobiotin-stained LMCs, we detected two distinct morphological types of LMCs in *P. xuthus* characterized by positions and shapes of axon terminals in the medulla and by the presence or absence of dendritic processes in the lamina (Fig. 1). Fig. 1A–E shows three LMCs with bushy terminals in the distal layer of the medulla; they are also characterized by dendritic processes covering all depths in the lamina. Although some of these LMCs (e.g. Fig. 1E) seemed to have longer processes than others (Fig. 1A,C), suggesting that they could represent two different cells types, no clear separation was possible because of small differences in the terminal depth (mean depth of 25±4 µm, n=6) and morphologically similar terminations. We designated such cells as L1/2.

Four neurobiotin-stained LMCs had terminals relatively deep in the medulla, at an average depth of 55±4 µm from the distal border

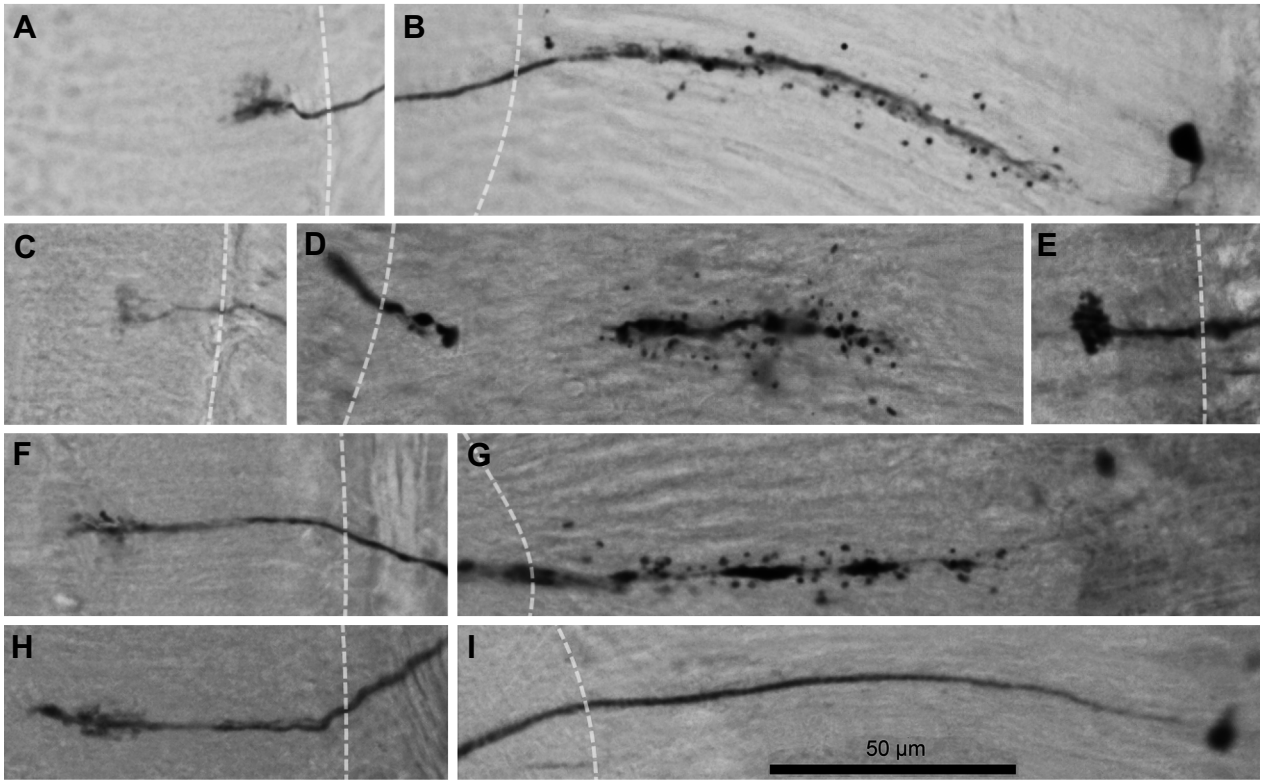

Fig. 1. Anatomical types of lamina monopolar cells (LMCs) in *Papilio xuthus*. Micrographs show LMCs with axons in the lamina (B,D,G,I) and terminals in the medulla (A,C,E,F,H). Image pairs A–B, C–D, F–G and H–I represent the same LMCs; for the LMC in E, only the image of the terminal is available. Dashed lines show the proximal border of the lamina in B,D,G,I, or the distal border of the medulla in A,C,E,F,H. Based on previous studies (Ribi, 1987), we classified LMCs in A–E as L1/2, and LMCs in F–I as L3/4.

Journal of Experimental Biology (2018) 221, jeb179085. doi:10.1242/jeb.179085

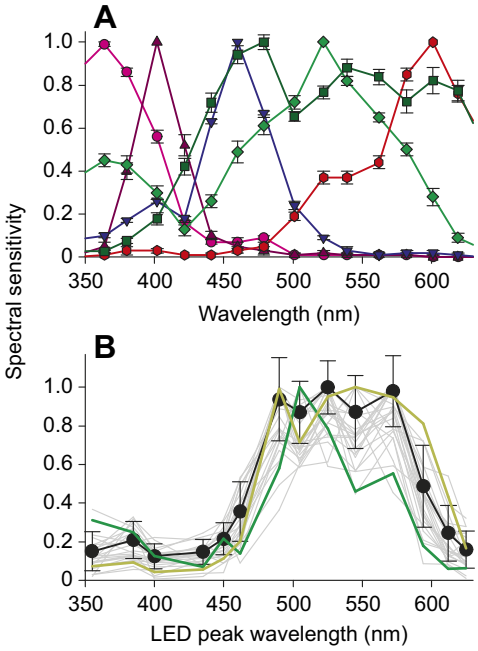

Fig. 2. Spectral sensitivity. (A) Average spectral sensitivity functions (SSFs) of *P. xuthus* photoreceptors; the plot is modified with permission from Arikawa (2003); here, error bars represent standard error of the mean. Green-sensitive, red-sensitive and broadband photoreceptors are the short visual fibers (SVFs) terminating in the lamina. (B) SSFs of individual LMCs are shown as thin gray traces; two dissimilar SSFs, a narrow and a wide one, are shown in green and yellow–green, respectively. The thick black trace is the average SSF; here and in all following figures, error bars represent standard deviation.

of the medulla (Fig. 1F,H). These LMCs had elongated bushy terminals. As shown in Fig. 1G,I, one such LMC had dendritic processes along the whole lamina, while another LMC lacked processes in the lamina. As it was possible that the lack of visible dendritic processes was due to poor staining, and because our sample size was small, it was not clear whether the cells belonged to different classes. We therefore designated such cells as L3/4.

Spectral sensitivity

Spectral sensitivity functions (SSFs) were obtained from 55 cells. Fig. 2 compares SSFs of different photoreceptors found in the compound eye of *P. xuthus* with those of LMCs. Photoreceptor SSFs (Fig. 2A) were reproduced from a previous study (Arikawa, 2003). Thin gray traces in Fig. 2B represent spectral sensitivity plots of 24 LMCs, for which the recordings were repeated at least twice (the traces are averages of two recordings). The black line in Fig. 2B indicates the average of all SSFs. In all these LMCs, the SSF maxima were situated between 490 and 572 nm. Most LMCs were characterized by very broad SSFs (e.g. thick yellow–green trace). On average, the half-width of SSFs equaled 118±14 nm (n=24). Although a minority of LMCs had relatively narrow SSFs (e.g. thick green trace), no statistical distinction could be made between the 'wide' and 'narrow' SSFs.

Light responses

Physiological responses of LMCs to light were investigated using 250 ms constant light pulses in dark-adapted butterflies (Fig. 3). LMCs responded with a characteristic hyperpolarization, probably mediated by opening of Cl^- channels as in flies (Hardie, 1989; Skingsley et al., 1995). Based on the presence of a depolarizing spike immediately after the termination of a hyperpolarizing voltage response ('off-spike'), two types of LMCs could be distinguished: spiking and non-spiking. A spike was defined as a transient depolarizing event with a minimal amplitude of 7.2 mV and a maximal half-width of 5.4 ms (see Materials and Methods for spike definition); 41 out of 67 recorded LMCs displayed spikes. Off-spike amplitude varied from cell to cell, reaching 50 mV in some LMCs; average off-spike amplitude was 21.8±11.6 mV (n=41). In these experiments, the average resting potential was −52±7.6 mV (n=41) in spiking cells and −48.3±8.5 mV in non-spiking cells (n=26; P=0.059, unpaired t-test). The maximal hyperpolarizing amplitude was 29±6.0 mV for spiking and 26.2±5.6 mV for non-spiking LMCs (P=0.073, unpaired t-test). However, these resting potentials were measured relative to an indifferent reference electrode in the extracellular space of the retina of the opposite eye and may not represent true membrane potentials (see Discussion).

Light responses shown in Fig. 3 were recorded from neurobiotin-stained LMCs presented in Fig. 1. Of six neurobiotin-stained L1/2 cells, three demonstrated no spikes at all (Fig. 3A), while three others showed relatively small off-spikes with an average amplitude of 11.4±3.3 mV (Fig. 3B). All neurobiotin-stained L3/4 cells showed prominent off-spikes with an average amplitude of 26.7±2.9 mV (n=4), and also spikes during light stimulation (Fig. 3C). The distribution of off-spike amplitudes shown in Fig. 3D indicates clustering around 15 and 30 mV.

To investigate the dependence of LMC hyperpolarization on light level, we used light pulses of different durations and intensities. Fig. 4A shows voltage responses of a typical spiking dark-adapted LMC to 250 ms light pulses at six light levels. Fig. 4B shows light

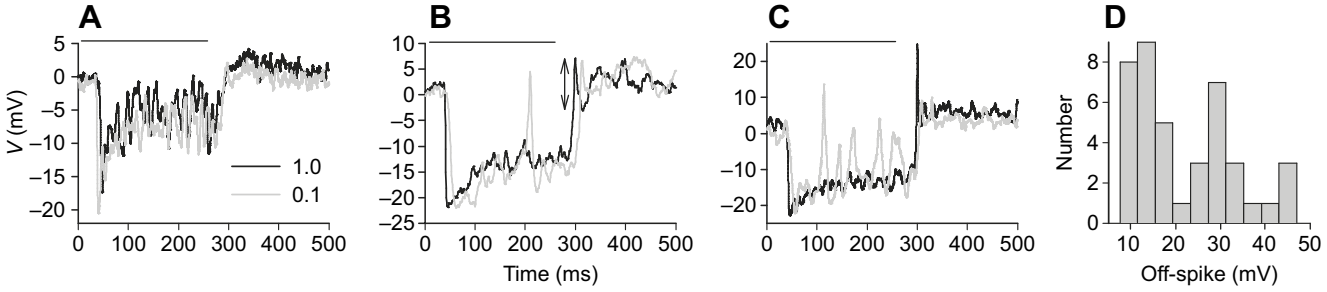

Fig. 3. Light response properties of the stained LMCs. (A–C) Voltage responses to 250 ms light pulses (horizontal lines). For each LMC, responses at two light intensities are presented: at an intensity where the LMC produced the highest amplitude off-spike [black traces, usually at neutral density (ND)2], and at a 10-fold lower light level (gray traces). (A) Recordings from the L1/2 cell shown in Fig. 1A,B. (B) Recordings from the L1/2 cell shown in Fig. 1C,D; the arrow indicates the off-spike amplitude. (C) Recordings from the L3/4 cell shown in Fig. 1F,G. (D) Distribution of off-spike amplitudes from 41 spiking LMCs; the off-spike amplitude threshold was 7.2 mV (see Materials and Methods).

Journal of Experimental Biology (2018) 221, jeb179085. doi:10.1242/jeb.179085

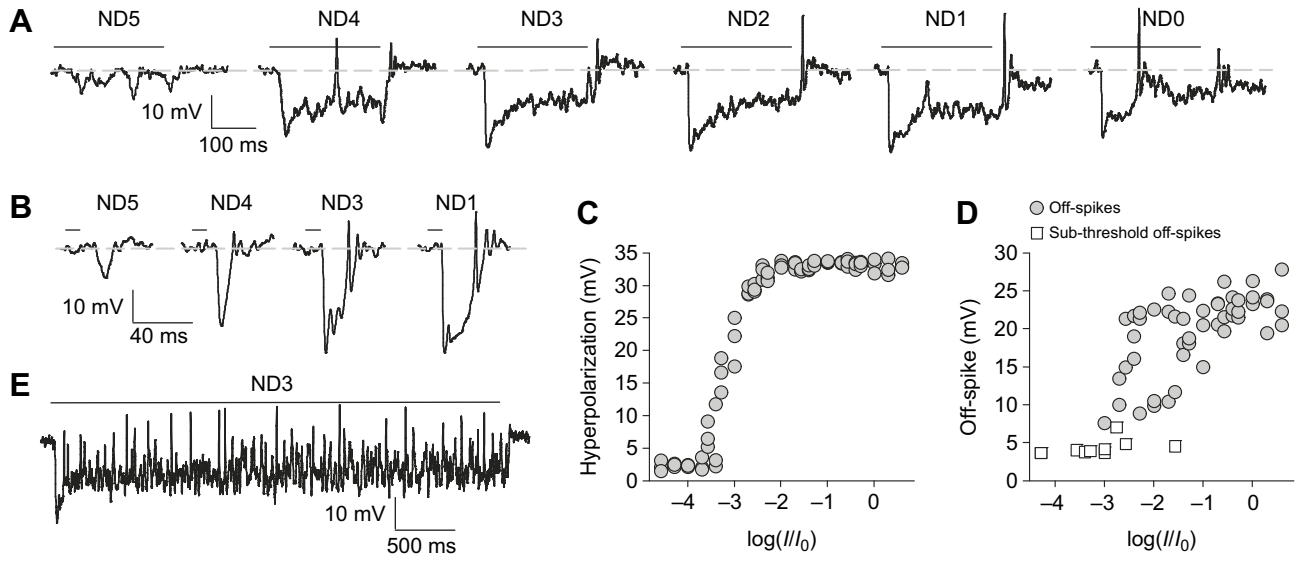

Fig. 4. Spiking in LMCs. (A) Typical responses of a spiking LMC to a 250 ms light stimulus at different light intensities (ND5–0). Horizontal bars (see also B and E) indicate the light stimulus; dashed gray lines (see also B) indicate the resting potential. (B) Responses of a different LMC to 10 ms pulses. (C) Dependence of hyperpolarization on light intensity for responses to the 10 ms stimulus over a 10^5 range of intensities (I; I_0, intensity of a non-attenuated stimulus). (D) Dependence of off-spike amplitudes on light intensity; small sub-threshold off-transients in dim light are shown as white squares, while 'regular' computer-detected spikes are shown as gray circles. Data in C and D were obtained from the LMC in B. (E) Sustained spiking during 4 s constant light stimulation in the dark.

responses of another typical spiking LMC to 10 ms light pulses at four light levels. In this LMC, the amplitude of hyperpolarization saturated relatively early (Fig. 4C), whereas off-spike amplitudes showed little saturation with increasing light intensity (Fig. 4D). In bright light, both sustained hyperpolarization and off-spike response amplitudes exhibited high variability from cell to cell.

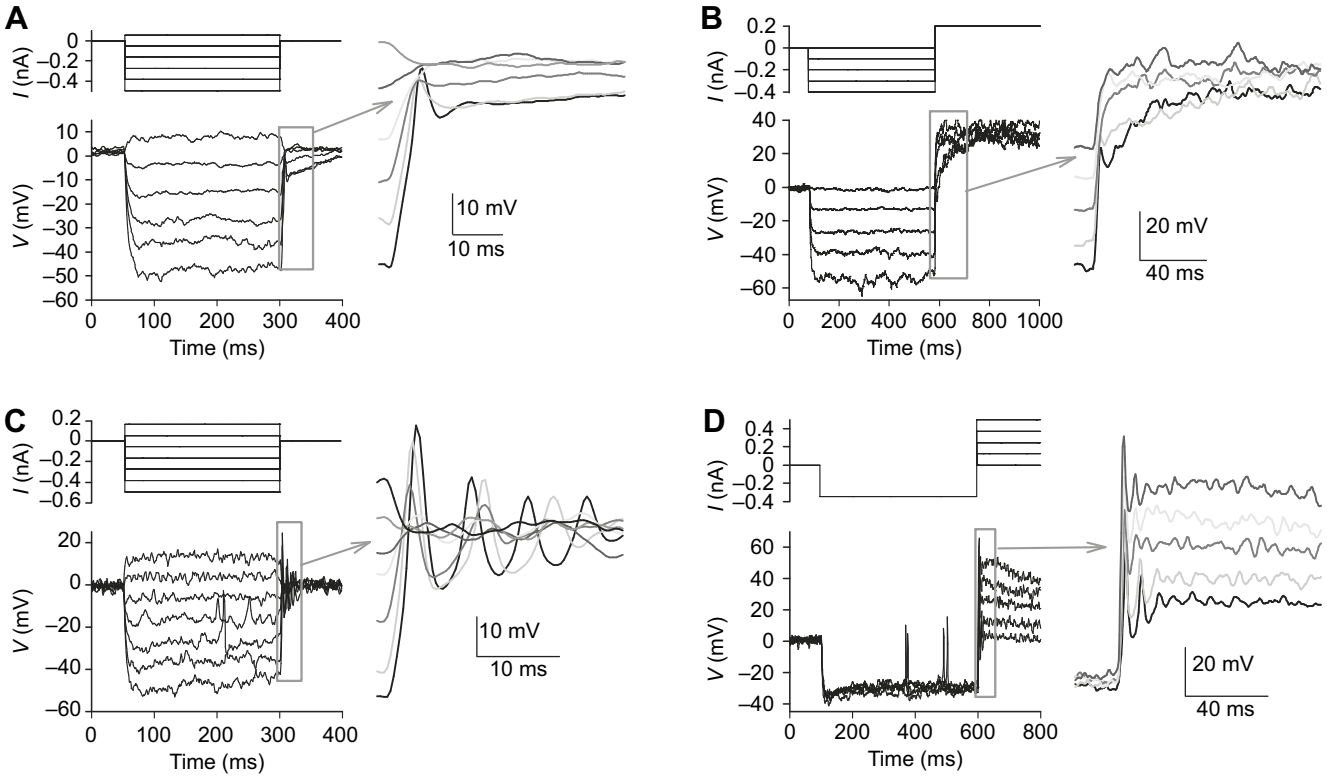

Fig. 5. Responses of LMCs to current injections in the dark. (A) Responses to a series of 250 ms current pulses; the stimulation protocol is shown above. Here and elsewhere, 0 mV indicates the resting potential. Inset to the right shows a magnified part of the response after the end of the current pulses. (B) Responses to a series of 500 ms current pulses (shown above), in −0.1 nA increments, followed by a 0.2 nA pulse. Inset to the right shows a magnified part of the response at the start of the depolarizing pulses. (C) Voltage responses to 250 ms current pulses (shown above) in the dark. Inset to the right shows oscillatory voltage responses after the end of strong hyperpolarizing current pulses. (D) Voltage responses to a stimulation protocol (shown above) consisting of 500 ms current pulses, in −0.4 nA increments, followed by a series of 500 ms current pulses, in 0.1 nA increments. Inset to the right shows membrane potential changes at the onset of the depolarizing testing pulses.

Journal of Experimental Biology (2018) 221, jeb179085. doi:10.1242/jeb.179085

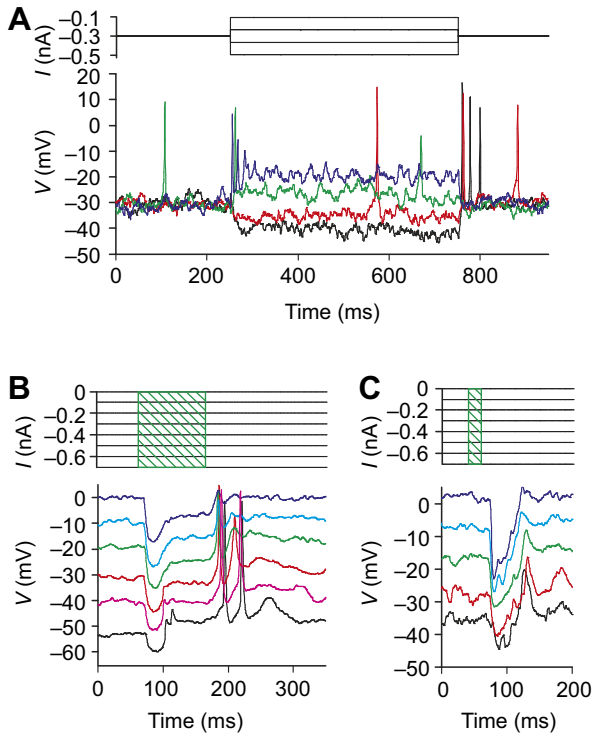

Fig. 6. Effects of hyperpolarization on spiking. (A) A spiking LMC was first hyperpolarized with a −0.3 nA injection and then additionally stimulated with 500 ms current pulses (shown above). (B) A spiking LMC was stimulated with 100 ms light pulses (green box above) of the same intensity during hyperpolarization by current pulses to different membrane potentials. (C) A non-spiking LMC was stimulated by 20 ms light pulses during hyperpolarization by current pulses.

In addition to off-spikes, which mark the transition from a hyperpolarized to a depolarized membrane potential at the end of either a light pulse or current injection, spikes could also be observed while the stimulus was on. Such 'on-spikes' appeared randomly and mainly in dim light (e.g. Fig. 4A, ND4 trace) and in some cells in the beginning of responses to bright light (e.g. Fig. 4A, ND0 trace). Such on-spikes tended to disappear rapidly during prolonged stimulation with bright light. Fig. 4D illustrates continuous generation of on-spikes during 4 s stimulation with constant light at ND3.

Analysis of spiking properties

We hypothesized that (1) spiking is mediated by a rapidly activating and inactivating depolarizing conductance, probably represented by Na_V channels as in the blowfly (Uusitalo et al., 1995); and that (2) non-spiking LMCs express fewer depolarizing channels than spiking LMCs. As our data suggested that spike generation depends on both hyperpolarization level and light intensity (Fig. 4A,C,D), it was necessary to separate these two factors. Therefore, we first investigated the properties of LMCs in the dark using positive (depolarizing) and negative (hyperpolarizing) current injections. We expected that if spiking is mediated by Na_V channels, then a substantial fraction of them would be inactivated at the normal resting potential of LMCs. When the cell is hyperpolarized, the inactivated channels would recover, with the extent of recovery depending on the amplitude and duration of hyperpolarization, which would be reflected in the properties of spikes evoked after depolarization to the resting potential.

We found prominent differences between responses of spiking and non-spiking LMCs to current injections. Responses of a typical non-spiking LMC to 250 ms current pulses are shown in Fig. 5. Although strong membrane hyperpolarizations failed to elicit spikes, relatively small spike-like events could be observed immediately after the end of the pulses, with their amplitudes increasing as hyperpolarization increased (Fig. 5A). However, usually these off-transients did not depolarize above the resting potential level (observed in six cells), and demonstrated slow-relaxing hyperpolarization after exposure to the most negative current pulses (Fig. 5A). Two non-spiking LMCs of this type were stained and identified as L1/2. These results indicate that (1) the depolarizing conductance does not play a major role in these off-transients and that (2) they might be mediated by a K^+ conductance similar to the fast-activating and inactivating A-type K^+ current in fly LMCs (Hardie and Weckström, 1990; Rusanen and Weckström, 2016).

Of 16 spiking LMCs recorded in our current injection experiments, three spiking LMCs were stained with neurobiotin. Two of them were identified as L3/4 and one as L1/2. Although spikes can be observed during hyperpolarizing current pulses, voltage responses after the termination of current injections were characterized by particularly robust and consistent depolarizing off-spikes sometimes exhibiting a slow-relaxing oscillatory behavior (Fig. 5C). The amplitude of depolarization and the number of spikes in the oscillatory train depended strongly on the magnitude of the preceding hyperpolarization (Fig. 5C). To determine whether increased depolarization changes the properties of off-spikes, we varied the amplitude of depolarizing current pulse applied after a 500 ms strongly hyperpolarizing current pulse (Fig. 5D). It can be seen that neither the amplitude nor the character of spike trains was substantially altered with depolarization (Fig. 5D). These results support the hypothesis that spikes are mediated by a depolarizing voltage-gated conductance.

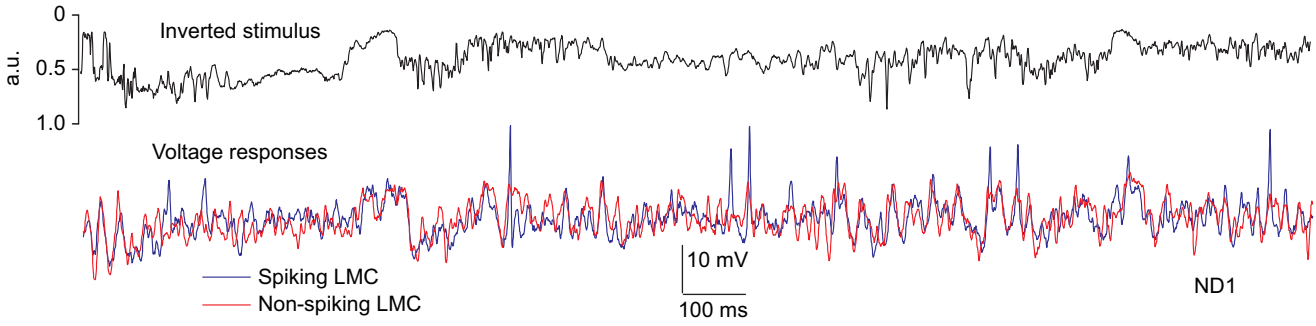

Fig. 7. Responses to naturalistic stimulation. Sections of responses (1 s duration) of a spiking (blue) and a non-spiking (red) LMC to 15 s naturalistic stimuli (NS; black trace above) obtained at the same light level, ND1. Responses were de-trended.

Journal of Experimental Biology (2018) 221, jeb179085. doi:10.1242/jeb.179085

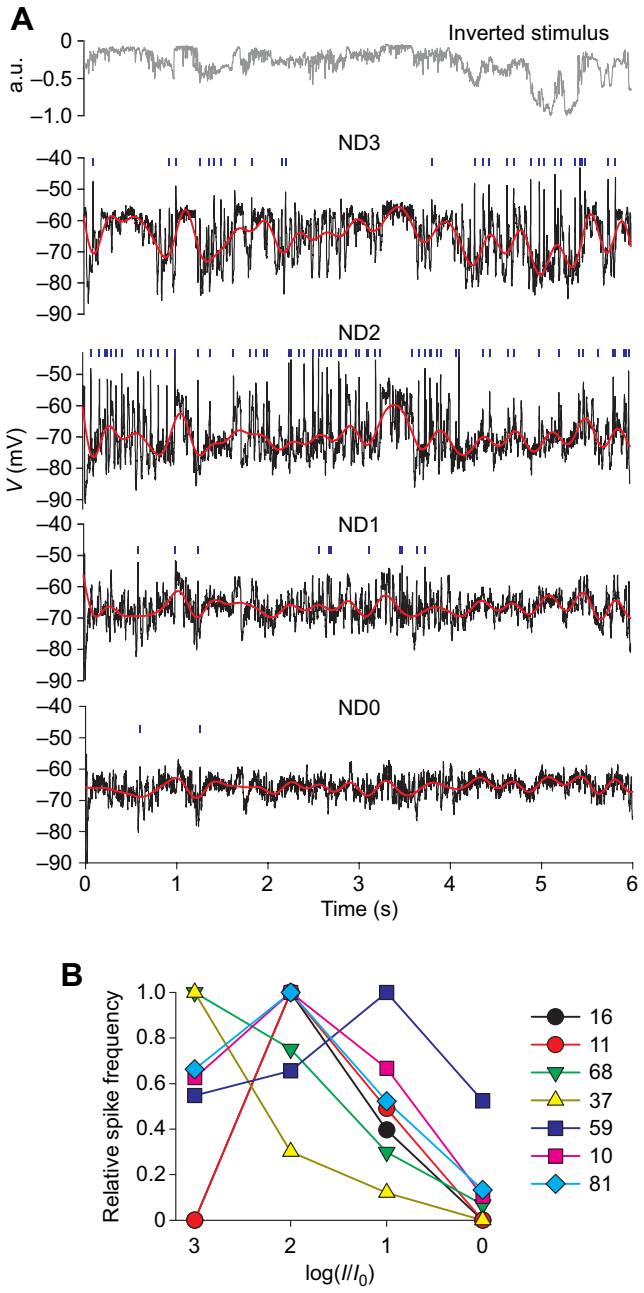

Fig. 8. Spiking cell responses to NS at different illumination levels. (A) Responses (6 s duration) to the same NS (shown above) at four light levels. The superimposed gray traces are trend lines obtained by low-pass filtering the response traces at a 3 dB cutoff frequency of 1 Hz; vertical bars above each trace indicate spikes. (B) Normalized dependency of mean spike rate on light intensity during 15 s of naturalistic stimulation are shown for seven LMCs; numbers in the key indicate the maximal number of spikes in each cell.

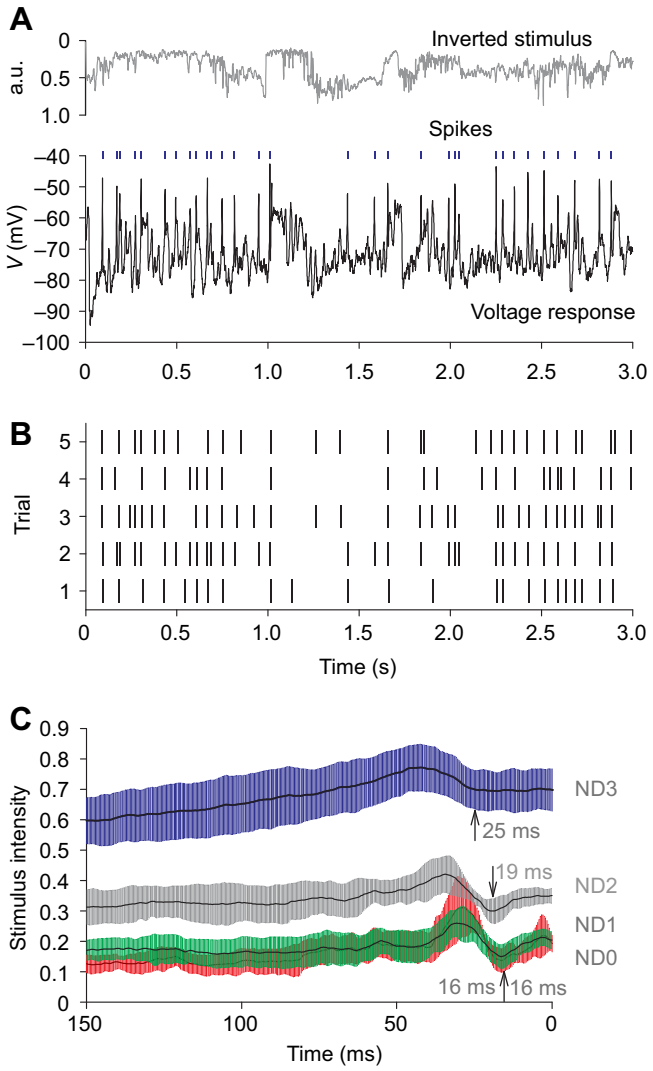

Fig. 9. Spikes accurately code stimulus features. (A) A 3 s section of a spiking LMC responses to NS at ND2; spikes (blue vertical bars above the trace) were detected using our computer-based algorithm. (B) A corresponding raster plot detailing positions of spikes (vertical bars) during five trials; spikes from the trace in A are shown in 'trial 2'. (C) Spike-triggered averages were obtained using five spiking cells stimulated with the same NS; error bars are s.d. The delay between stimulus onset and the LMC voltage response was determined by cross-correlating the stimulus and voltage-response traces. The values in colour are average lags, indicating the onset of spike.

Moreover, the presence of transient hyperpolarization seen at the onset of depolarizing pulses (Fig. 5D) suggests that spiking LMCs might also express A-type K^+ current. Overall, spiking LMCs were characterized by high variability in off-spike amplitude, presence or absence of spike oscillations, dependency of spiking on membrane potential, and the size of the putative A-type K^+ conductance.

Above, we focused on off-spikes evoked when membrane voltage returned to the resting (Fig. 5C) or a depolarized (Fig. 5D) state after a hyperpolarization. However, in six cells we observed spontaneous on-spikes during current pulses. These on-spikes did not occur randomly at any hyperpolarized potential. Instead, they were restricted to a relatively small voltage window of about 20–40 mV below the resting potential (Fig. 5C). In the experiment shown in Fig. 6, a spiking LMC was first hyperpolarized with a continuous 1 s, −0.3 nA pre-pulse and then, in the middle of current injection, stimulated using additional current pulses to further hyperpolarize or depolarize the membrane. No on-spikes were evoked during the most hyperpolarizing current pulse (black trace in Fig. 6A). Spikes were reliably elicited at the beginning of small depolarizing pulses (blue and green traces) and after hyperpolarizing current pulses (red and black traces).

We also tested the effects of hyperpolarization in combination with light stimulation on spike generation (Fig. 6B). Although the amplitude of light-induced hyperpolarization decreased strongly with increased background hyperpolarization, up to the point of virtual

Journal of Experimental Biology (2018) 221, jeb179085. doi:10.1242/jeb.179085

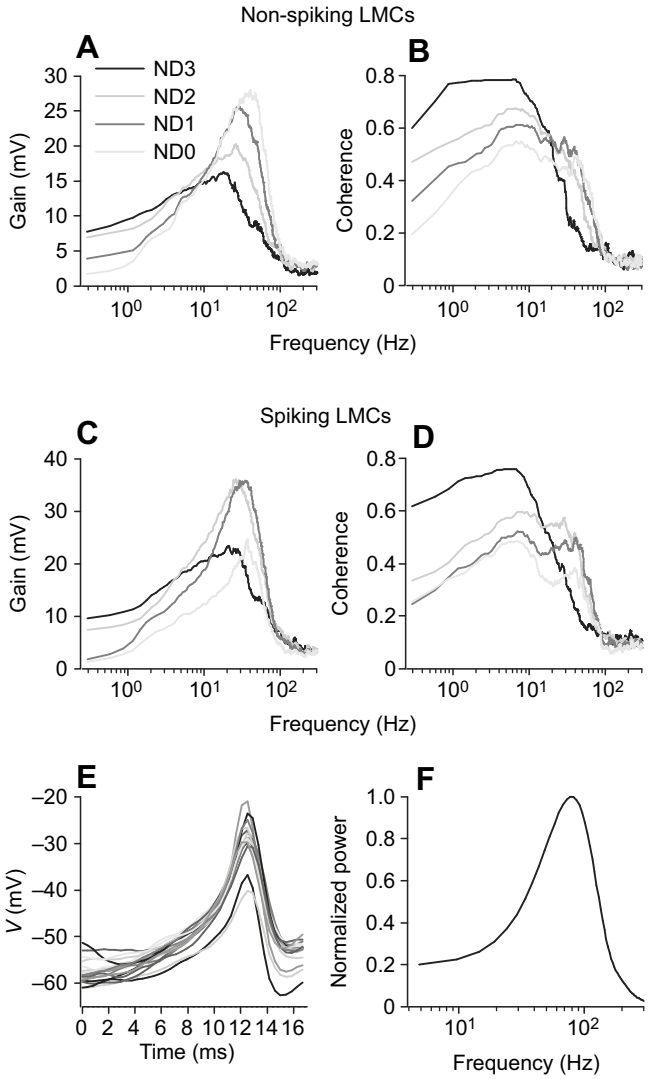

Fig. 10. Gain and coherence functions. (A–D) Average gain (A,C) and coherence (B,D) functions of five non-spiking (A,B) and five spiking (C,D) LMCs at four backgrounds as indicated. (E) Nineteen different spikes extracted from a NS response. (F) Normalized average power spectrum of the spikes shown in E.

disappearance of the sustained voltage response component (Fig. 6B, pink and black traces), off-spikes continued to increase in amplitude. While off-transients were small in the non-spiking LMCs, they also tended to increase with hyperpolarization (Fig. 6C).

Spikes and naturalistic stimulation

To investigate whether spikes are involved in information processing, we recorded responses to NS (see Materials and Methods) from a total of 23 LMCs, including 14 spiking and nine non-spiking LMC: six of these 23 neurons were successfully stained with neurobiotin, two were classified as L3/4 and spiked in response to NS, and four were L1/2 and did not spike.

One of two NS lasting 15 s, was repeated 5 times at each of four illumination levels: ND3–ND0. Nine cells responded to the NS with a combination of graded potentials and spikes, with the number of spikes varying from three to 81 during the 15 s recordings. A 1 s section of the NS with typical responses of spiking and non-spiking LMCs is shown in Fig. 7. In the following analysis we used only LMCs that produced at least 10 spikes during 15 s naturalistic stimulation.

Fig. 8 shows 7 s fragments of a spiking LMC response to 15 s NS at four light levels. At the two lowest illumination levels (Fig. 8A, ND3, ND2) the membrane potential reliably followed slow changes in stimulus intensity and reached more hyperpolarized potentials than at brighter illuminations (ND1, ND0). The number of spikes generated by a LMC and detected by our computer-based algorithm depended strongly on the general illumination level. The spikes (vertical bars above the response) were larger in dimmer than in brighter light: on average, detected spikes were 32% smaller at the highest intensity level (Fig. 8A, ND0) than in dim light, where the largest spikes were found (Fig. 8A, ND3). Fig. 8B shows the dependency of the mean spike count during 15 s recordings on light intensity for seven LMCs.

Are the spikes stochastic events or are they triggered by certain aspects of the stimulus? We compared spike sequences from five repetitions of a LMC response to the same NS under the same conditions. Fig. 9A shows a 3 s fragment of one such response, and Fig. 9B shows a raster plot of the corresponding spike events from all five repeats. This direct comparison indicates that the positions of spikes in the spike train are reproduced quite accurately from trial to trial.

Therefore, it was necessary to determine which specific aspects of the NS cause spikes and whether they are similar for all light intensities. For this, we computed STAs by aligning and averaging the fragments of the stimulus preceding each spike in the response. Fig. 9C shows STA functions computed at four backgrounds (ND3–ND0). The functions were quite similar, with stimulus intensity first increasing, then reaching a peak, and then decreasing again. A spike was initiated shortly after the peak (arrows). This sequence corresponds to the initial hyperpolarization of a LMC, which would probably recover a fraction of depolarization-activated channels from inactivation, followed by depolarization, which triggers concerted opening of these and other available depolarizing channels. However, there were differences between the backgrounds, as in bright light the mean intensity preceding the spike was relatively low, and a drastic intensity change was needed to trigger a spike. In dim light, in contrast, the mean stimulus intensity was relatively high, and a smaller intensity change was needed to elicit a spike.

Transfer functions

The natural stimuli and the LMC responses they evoked were Fourier transformed and processed to derive response gain and coherence as a function of frequency (see Materials and Methods). The functions obtained from five non-spiking and five spiking LMCs at each light intensity are plotted, as averages, in Fig. 10. Gain functions demonstrated band-pass filtering at all light levels, and especially in bright light. The maximal corner frequencies were 63.0±7.8 Hz for the non-spiking and 54.8±5.4 Hz for the spiking LMCs (P=0.099, unpaired t-test).

The most striking differences between spiking and non-spiking LMCs were found in the coherence function, which is a measure of linearity and noise content of an information-transmission system. Coherence functions for the spiking LMCs showed clear local minima at the three brightest backgrounds between 10 and 20 Hz, which indicates the presence of a localized non-linearity or relatively high noise in this frequency band (Fig. 10D).

DISCUSSION

LMCs and their vertebrate counterparts, the bipolar cells, were long regarded as non-spiking neurons, exclusively relying on graded potentials in information transfer. However, as now established in vertebrates, graded-to-spiking conversion begins in the axons of

bipolar cells (Baden et al., 2013). In insects, previous research suggested that spiking is an important aspect of LMC signaling (Järvilehto and Zettler, 1971; Zettler and Järvilehto, 1971, 1971; Hardie and Weckström, 1990; Rusanen et al., 2017; Hardie and Weckström, 1990; Rusanen and Weckström, 2016). Our recordings from the LMCs of the butterfly *P. xuthus* provide further evidence that LMCs use spike-like events to emphasize light intensity decrements. Below, we discuss our main findings and their implications.

Spectral sensitivity

Are LMCs in *P. xuthus* involved in chromatic vision? Among photoreceptors in the compound eye of the butterfly, LVFs R1 and R2 are UV, violet or blue sensitive, whereas SVFs (R3–R8) are green sensitive, red sensitive or broadband photoreceptors (Hamanaka et al., 2013; Arikawa, 2003). Ommatidia are classified into three different types according to the specific SVFs and LVFs they contain. All ommatidia contain two green-sensitive R3 and R4 photoreceptors, with R6 and R8 red-sensitive photoreceptors in type 1, broadband photoreceptors in type 2, and green-sensitive photoreceptors in type 3 ommatidia.

We show that in terms of spectral sensitivity, the majority of LMCs in *P. xuthus* appear to receive mixed input from long-wavelength photoreceptors of different types, resulting in broad SSFs. This suggests that information from photoreceptors of different spectral types might be used in the processing of motion-related signals (Hardie, 1985; Wardill et al., 2012). Such integration would increase the spectral bandwidth of the photon catch and improve absolute sensitivity, which is particularly important for achromatic vision in dim light.

However, it was found that green- and red-sensitive photoreceptors (SVFs contacting with LMCs in the lamina) contribute to color discrimination. This suggests that the LMCs relaying signals from such photoreceptors could be involved in color vision. Moreover, some LMCs demonstrated narrow SSFs (e.g. Fig. 2B, green trace), implying that they receive inputs mainly from photoreceptors of specific spectral classes and thus contribute to chromatic vision. Spectral-opponent LMCs as reported in the worker honeybee and dragonfly (de Souza et al., 1992; Yang and Osorio, 1996) were not reliably detected in *P. xuthus*. Although we recorded spectral-opponent responses from several cells, with shorter wavelength light pulses causing depolarizations and longer wavelength pulses causing hyperpolarizations, we were not able to establish with certainty that they were made from LMCs because of the instability of such recordings.

Spiking and non-spiking LMCs

We describe two morphologically and electrophysiologically different types of LMCs. LMCs terminating near the surface of the medulla with roundish terminals were designated as L1/2, whereas LMCs terminating in a much deeper layer with elongated terminals were classified as L3/4, in accordance with the previous descriptions of LMCs in *Papilio* (Ribi, 1987; Hamanaka et al., 2013). We show that L1/2 and L3/4 appear to have distinct electrophysiological properties. Specifically, all L3/4 produced off-spikes of high amplitude, while L1/2 showed much smaller off-transients. Similar results were obtained in naturalistic stimulation experiments, where on-spikes were detected in L3/4 cells exclusively. However, because of small sample sizes, our classification is necessarily tentative, with the main uncertainty being the validity of L1/2 classification because some of such cells demonstrated small spikes.

Our analysis of off-transients in non-spiking L1/2 cells indicated that they are mainly caused by a transient voltage-activated K^+ conductance, which resembles the A-type conductance found in LMCs of the locust and several Diptera species (Weckström et al., 1991; Benkenstein et al., 1999; Skingsley et al., 1995); evidence of such a conductance was also found in spiking LMCs (Fig. 5). Our data suggest that the repolarizing K^+ conductance has an activation threshold below resting potential and is partly inactivated at rest. Inactivation of these channels is relieved in a time- and voltage-dependent manner during hyperpolarization, so that they can open again at the onset of consecutive depolarization and transiently hyperpolarize the membrane. Slow relaxation of this secondary hyperpolarization could be caused by gradual inactivation of these channels. However, light responses recorded at highly hyperpolarized potentials also revealed a small depolarizing conductance as evidenced by the presence of transient depolarization after the end of light pulses (Fig. 6C, green, red and black traces), implying that putative Na_V channels may not be completely absent in non-spiking LMCs.

Therefore, both spiking and non-spiking LMCs appear to express Na_V and A-type K^+ channels, differing only in the levels of channel expression. This is consistent with previous observations in blowflies, where spikes in L1 and L3 cells were abolished by inhibiting Na_V channels (Uusitalo et al., 1995). The evidence supporting the Na_V hypothesis was found in the inactivation removal experiments (Figs 5 and 6). The depolarizing channels were mainly inactivated at resting potential, as, upon gradual removal of inactivation by light- or current-induced hyperpolarization, the off-spike amplitudes increased up to the point of generating what can only be described as action potentials (Fig. 6B, black trace). These ‘spikes’ were characterized by high amplitudes, over 40 mV, and by extremely short times to peak, of the order of milliseconds. No other ion channels except Na_V can generate such responses. It also appears that the activation threshold for the putative Na_V channels is below resting potential, because off-spikes could be produced after hyperpolarizing current injections by membrane depolarizations to or below resting potential (Figs 5 and 6).

However, membrane potentials measured intracellularly in LMCs are most likely not true measures of LMC membrane potential because they were recorded with respect to a distant reference point, retinal extracellular space. Experiments on flies showed that in the dark-adapted animal the lamina extracellular space is approximately 30 mV negative with respect to the retinal extracellular space (Weckström and Laughlin, 2010). As a result, the true LMC membrane potential in the butterfly lamina can be tens of millivolts more positive than the recorded potential. This and other uncertainties, such as the unknown localization of the putative Na_V channels, prevent us from specifying the voltage ranges for activation and inactivation of the conductances discussed here.

It is not known why some LMCs, such as L3/4, generate spikes, while others, such as L1/2, do not. However, spiking and non-spiking LMC types have been observed in other species too (de Souza et al., 1992; Uusitalo et al., 1995; Rusanen et al., 2017). In *Drosophila*, it was shown that L1–L3 made distinct contributions to contrast detection and color vision (Arenz et al., 2017; Melnattur et al., 2014; Tuthill et al., 2013; Silies et al., 2013; Joesch et al., 2010; Gao et al., 2008).

Spiking at different backgrounds

Although we have shown that spike rate decreases with illumination intensity, this relates to large distinct spikes, which were detectable

with our template-based computer algorithm. It is apparent from Fig. 8 that the size of depolarizing transients becomes smaller with increasing stimulus brightness, leading to progressive disappearance of above-threshold transients. What mechanism could explain these observations?

Photoreceptors in flies adjust their transfer function according to light intensity, with band-pass filtering becoming more prominent in bright light (Hardie and Postma, 2009). Further modulation takes place at the photoreceptor–LMC synapse (Juusola et al., 1996). In dim light, presynaptic gain is high at low frequencies, yielding increased amplification of slow changes in stimulus brightness. At the level of LMCs, this translates into a variable response baseline (Fig. 8A, gray trend lines), large hyperpolarizing aspects of which help recovery of the putative Na_V channels from inactivation. Consecutive depolarizations trigger spikes. The larger and the longer the hyperpolarization, the higher the spike amplitude can become. In contrast, in bright light, the gain in the low-frequency region decreases, producing LMC responses with relatively low baseline variability. In the absence of large hyperpolarizations, the putative Na_V channels stay mainly inactivated, do not generate large spikes, and instead contribute to amplification of small depolarizing features of the response. Nonetheless, detectable spikes can be produced even in bright light, albeit this requires faster and larger changes in stimulus amplitude, as evidenced by the differences between STA functions at different backgrounds (Fig. 9C).

We have shown that spikes can be reproduced quite reliably from trial to trial in naturalistic stimulation experiments (Fig. 9B). However, when one compares the patterns of spike trains at the two backgrounds (ND2 and ND3) in dim light (Fig. 8A), they appear to be quite dissimilar, so that the same contrast sequence that produces many spikes at one intensity can elicit almost no spikes at another light level and vice versa. At least two mechanisms could account for this discrepancy. First, as described above, different light backgrounds can result in different LMC hyperpolarization levels, with dissimilar effects on the availability of Na_V channels and their activation patterns. Second, light adaptation in photoreceptors alters quantum bump amplitude, which determines the bump noise level, and also membrane time constant, which limits the resolution of fast temporal changes (Frolov et al., 2017). Even in the absence of instrumental noise, dissimilar photoreceptor adaptation states would inevitably alter the fine pattern of the LMC response, which is crucial for spike generation.

Non-linear amplification

By introducing additional elements of non-linearity between the transduced naturalistic signal and LMC response, the putative Na_V conductance dramatically alters the coherence functions (Fig. 10B,D). This was observed not only in the relatively dim backgrounds where distinct spikes could be detected but also at the brightest light level, when spikes became too small to be detected. We hypothesized that coherence function minima are caused by the spikes, which non-linearly amplify decreases in light intensity, or, as in bright light, by depolarizing transients not detected as spikes. However, as can be seen from Fig. 10E,F, computer-detected spikes were characterized by power spectra with maxima around 80 Hz, which is much higher than the frequencies of coherence function minima (Fig. 10D). Therefore, the source of the non-linearity is likely to be the smaller but ubiquitous spikelets, which could not be detected by our algorithm. Thus, although large spikes disappeared, the non-linearity due to the ubiquitous contribution of the putative Na_V channels to the amplification of depolarizing transients persisted. It should be noted that these channels may have an additional role in the amplification of hyperpolarizing transients associated with increases in light intensity. Membrane hyperpolarization would rapidly deactivate channels that were open at rest and increase membrane resistance, and this increase in resistance would passively amplify hyperpolarizing components of the stimulus. The A-type conductance might also be involved in such signal amplification.

Therefore, the putative Na_V channels can selectively modify voltage signals, producing an amplifying resonance that depends on the channel kinetics (Hutcheon and Yarom, 2000). The function of these channels (in combination with the A-type current) in bright light could be to increase voltage gain at around 20 Hz by amplifying responses and making them more transient.

One could argue that, apart from purely biophysical reasons, large spikes are not used in bright light because they would lower the information rate as each spike replaces an information-rich graded voltage signal (de Ruyter van Steveninck and Laughlin 1996; Juusola and French, 1997; Kretzberg et al., 2001), or because the spikes are overly costly (Laughlin et al., 1998). In contrast, large spikes resembling action potentials can be used under dim-light conditions where such concerns would be less problematic, because, as a result of the strong presynaptic low-pass filtering, the signal received by the LMC contains only relatively slow frequencies. In other words, in dim light 'spike coding' is separated from the 'analog coding' in the frequency domain (Fig. 10D, black trace, Fig. 10F). Encoding prominent events, i.e. fast and large contrast decrements, with all-or-none spikes would protect them against attenuation and intrinsic noise, and probably cause a large response in the postsynaptic cell. As in dim light the spikes are of the all-or-none type and reproduced accurately, one could hypothesize that their role is to encode temporal locations of prominent events rather than to provide exact information about contrast magnitude. It should also be noted that because the light source had an angular size of 6–7°C, stimulation did not fully recruit the antagonistic surround of the LMCs and, as a result, the cells were more strongly hyperpolarized than they would be if the stimulus was panoramic. Thus, the reduction in on-spiking observed at bright backgrounds might be greater with our stimulus than occurs in nature when, as is normally the case, extended scenes fully recruit the surround.

Conclusions

The following functional scenario is suggested for the spiking LMCs. In dim light, because of the sign-inverting character of LMC response, spiking is used to amplify decreases in light intensity, which are encoded by depolarizations. Spikes are superimposed on the graded potential, which more or less reliably reproduces the photoreceptor response. In brighter light, the gain of LMCs decreases in the low-frequency part of the spectrum, and the LMCs acquire band-pass filtering properties (Fig. 10A,C). As a result of reduced variability in the response baseline, patterns of the putative Na_V channel kinetics change, leading to the disappearance of large spikes. While it can be assumed that spiking alters information transfer, we were not able to evaluate its added value because of the inadequacy of existing methods of information rate calculations, which do not allow reliable estimation of information transfer when both graded and action potentials (or spikes) are used by the neuron. For instance, if a coherence-based method (Ibrahim, 1993) was used, then under otherwise equal conditions it would provide a smaller information rate estimate for a spiking than for a non-spiking LMC, because spiking disrupts the coherence function. If, however, an entropy method (French and Pfeiffer, 2011) was considered, then a question arises as to whether to treat spikes as all-or-none events, with no information encoded in the amplitude, or as graded potentials.

Therefore, the signaling strategy of spiking LMCs changes according to the light level: in dim light, graded signals and large spikes are used without mutual interference as the channels are separated in the frequency domain; in bright light, graded potentials amplified by a resonance band created by the putative Na_V channels are used.

Importantly, our findings demonstrate that the flow of information from the periphery to the center is accompanied not by an abrupt but by a gradual development of spiking capacity along the sensory pathway. As information from photoreceptors to LMCs is transferred almost exclusively by means of graded signals (but see action potentials observed in the axons of the honey bee drone and American cockroach; Vallet et al., 1992; Heimonen et al., 2006), a large fraction of LMCs already show prominent involvement of the putative Na_V channels in signal processing. Spikes elicited by these channels are used to amplify sharp intensity decrements and, possibly, also intensity increments as suggested above. However, probably as a result of the low density of Na_V channel expression, action potential-like events are observed rarely, after prolonged hyperpolarizations that could maximally recover Na_V channels from inactivation. It would be expected that at the next relay, the medullar interneurons, coding with action potentials, would begin in earnest but coding by graded signals would also persist to some extent as observed in the locust (Osorio, 1987a,b). This highlights the necessity to develop new information calculation methods that would allow reliable estimation of information transfer by mixed action potential and graded voltage signals (e.g. Sengupta et al., 2014).

Acknowledgements
The authors thank Prof. Andrew S. French for proofreading of the manuscript.

Competing interests
The authors declare no competing or financial interests.

Author contributions
Conceptualization: J.R., M.T.W., M.K., K.A.; Methodology: J.R., K.A.; Validation: J.R., R.V.F.; Formal analysis: J.R.; Investigation: J.R., M.K.; Resources: M.K.; Writing - original draft: J.R.; Writing - review & editing: J.R., R.V.F., K.A.; Supervision: R.V.F., K.A.; Funding acquisition: K.A.

Funding
This research received no specific grant from any funding agency in the public, commercial or not-for-profit sectors.

References
Arenz, A., Drews, M. S., Richter, F. G., Ammer, G. and Borst, A. (2017). The temporal tuning of the *Drosophila* motion detectors is determined by the dynamics of their input elements. *Curr. Biol.* **27**, 929-944.
Arikawa, K. (2003). Spectral organization of the eye of a butterfly, *Papilio*. *J Comp Physiol A* **189**, 791-800.
Baden, T., Euler, T., Weckström, M. and Lagnado, L. (2013). Spikes and ribbon synapses in early vision. *Trends Neurosci.* **36**, 480-488.
Benkenstein, C., Schmidt, M. and Gewecke, M. (1999). Voltage-activated whole-cell K+ currents in lamina cells of the desert locust Schistocerca gregaria. *J. Exp. Biol.* **202**, 1939-1951.
de Ruyter van Steveninck, R. R. and Laughlin, S. B. (1996). The rate of information transfer at graded-potential synapses. *Nature* **379**, 642-645.
de Souza, J., Hertel, H., Ventura, D. F. and Menzel, R. (1992). Response properties of stained monopolar cells in the honeybee lamina. *J Comp Physiol A* **170**, 267-274.
French, A. S. and Pfeiffer, K. (2011). Measuring entropy in continuous and digitally filtered neural signals. *J. Neurosci. Methods* **196**, 81-87.
Frolov, R. V., Matsushita, A. and Arikawa, K. (2017). Not flying blind: a comparative study of photoreceptor function in flying and non-flying cockroaches. *J. Exp. Biol.* **220**, 2335-2344.
Gao, S., Takemura, S., Ting, C., Huang, S., Lu, Z., Luan, H., Rister, J., Thum, A. S., Yang, M., Hong, S. et al. (2008). The neural substrate of spectral preference in *Drosophila*. *Neuron* **60**, 328-342.
Hamanaka, Y., Shibasaki, H., Kinoshita, M. and Arikawa, K. (2013). Neurons innervating the lamina in the butterfly, Papilio xuthus. *J Comp Physiol A* **199**, 341-351.
Hardie, R. C. (1985). Functional organization of the fly retina. In *Progress in Sensory Physiology* (ed. H. Autrum, D. Ottoson, E. R. Perl, R. F. Schmidt, H. Shimazu and W. D. Willis), pp. 1-79. Berlin, Heidelberg: Springer.
Hardie, R. C. (1989). A histamine-activated chloride channel involved in neurotransmission at a photoreceptor synapse. *Nature* **339**, 704-706.
Hardie, R. and Postma, M. (2009). Phototransduction in microvillar photoreceptors of drosophila and other invertebrates. In *The Senses: a Comprehensive Reference: Vision I* (ed. R. H. A. T. Masland), pp. 77-130. Oxford: Academic Press.
Hardie, R. C. and Weckström, M. (1990). Three classes of potassium channels in large monopolar cells of the blowfly *Calliphora vicina*. *J Comp Physiol A* **167**, 723-736.
Heimonen, K., Salmela, I., Kontiokari, P. and Weckström, M. (2006). Large functional variability in cockroach photoreceptors: optimization to low light levels. *J. Neurosci.* **26**, 13454-13462.
Heisenberg, M. and Buchner, E. (1977). The role of retinula cell types in visual behavior of *Drosophila melanogaster*. *J Comp Physiol A* **117**, 127-162.
Hutcheon, B. and Yarom, Y. (2000). Resonance, oscillation and the intrinsic frequency preferences of neurons. *Trends Neurosci.* **23**, 216-222.
Ibrahim, R. A. (1993). Engineering applications of correlation and spectral analysis-Julius S. Bendat and Allan G. Piersol. *AIAA J.* **31**, 2190-2191.
Järvilehto, M. and Zettler, F. (1971). Localized intracellular potentials from pre- and postsynaptic components in the external plexiform layer of an insect retina. *Z vergl Physiol* **75**, 422-440.
Joesch, M., Schnell, B., Raghu, S. V., Reiff, D. F. and Borst, A. (2010). ON and OFF pathways in *Drosophila* motion vision. *Nature* **468**, 300-304.
Juusola, M. and French, A. S. (1997). The efficiency of sensory information coding by mechanoreceptor neurons. *Neuron* **18**, 959-968.
Juusola, M., French, A. S., Uusitalo, R. O. and Weckström, M. (1996). Information processing by graded-potential transmission through tonically active synapses. *Trends Neurosci.* **19**, 292-297.
Kretzberg, J., Warzecha, A. K. and Egelhaaf, M. (2001). Neural coding with graded membrane potential changes and spikes. *J. Comput. Neurosci.* **11**, 153-164.
Laughlin, S. (2010). Optic lamina of fast flying insects as a guide to neural circuit design-Oxford Medicine. In *Handbook of Brain Microcircuits* (ed. Shepherd and Gordon), pp. 404-414. Oxford: Oxford University Press.
Laughlin, S. B. and Osorio, D. (1989). Mechanisms for neural signal enhancement in the blowfly compound Eye. *J. Exp. Biol.* **144**, 113-146.
Laughlin, S. B., de Ruyter van Steveninck, R. R. and Anderson, J. C. (1998). The metabolic cost of neural information. *Nat. Neurosci.* **1**, 36-41.
Melnattur, K. V., Pursley, R., Lin, T.-Y., Ting, C.-Y., Smith, P. D., Pohida, T. and Lee, C.-H. (2014). Multiple redundant medulla projection neurons mediate color vision in *Drosophila*. *J. Neurogenet.* **28**, 374-388.
Osorio, D. (1987a). Temporal and spectral properties of sustaining cells in the medulla of the locust. *J Comp Physiol A* **161**, 441-448.
Osorio, D. (1987b). The temporal properties of non-linear, transient cells in the locust medulla. *J Comp Physiol A* **161**, 431-440.
Ribi, W. A. (1987). Anatomical identification of spectral receptor types in the retina and lamina of the Australian orchard butterfly, *Papilio aegeus* D. *Cell Tissue Res.* **247**, 393-407.
Rusanen, J. and Weckström, M. (2016). Frequency-selective transmission of graded signals in large monopolar neurons of blowfly *Calliphora vicina* compound eye. *J. Neurophysiol.* **115**, 2052-2064.
Rusanen, J., Vähäkainu, A., Weckström, M. and Arikawa, K. (2017). Characterization of the first-order visual interneurons in the visual system of the bumblebee (Bombus terrestris). *J Comp Physiol A* **203**, 903-913.
Sengupta, B., Laughlin, S. B. and Niven, J. E. (2014). Consequences of converting graded to action potentials upon neural information coding and energy efficiency. *PLoS Comput. Biol.* **10**, e1003439.
Silies, M., Gohl, D. M., Fisher, Y. E., Freifeld, L., Clark, D. A. and Clandinin, T. R. (2013). Modular use of peripheral input channels tunes motion-detecting circuitry. *Neuron* **79**, 111-127.
Skingsley, D. R., Laughlin, S. B. and Hardie, R. C. (1995). Properties of histamine-activated chloride channels in the large monopolar cells of the dipteran compound eye: a comparative study. *J Comp Physiol A* **176**, 611-623.
Takemura, S. and Arikawa, K. (2006). Ommatidial type-specific interphotoreceptor connections in the lamina of the swallowtail butterfly, Papilio xuthus. *J. Comp. Neurol.* **494**, 663-672.
Takemura, S., Kinoshita, M. and Arikawa, K. (2005). Photoreceptor projection reveals heterogeneity of lamina cartridges in the visual system of the Japanese yellow swallowtail butterfly, *Papilio xuthus*. *J. Comp. Neurol.* **483**, 341-350.
Tuthill, J., Nern, A., Holtz, S., Rubin, G. and Reiser, M. (2013). Contributions of the 12 neuron classes in the fly lamina to motion vision. *Neuron* **79**, 128-140.
Uusitalo, R. O., Juusola, M. and Weckström, M. (1995). Graded responses and spiking properties of identified first-order visual interneurons of the fly compound eye. *J. Neurophysiol.* **73**, 1782-1792.
Vallet, A. M., Coles, J. A., Eilbeck, J. C. and Scott, A. C. (1992). Membrane conductances involved in amplification of small signals by sodium-channels in photoreceptors of drone honey bee. *J. Physiol.* **456**, 303-324.

van Hateren, J. H. (1992). A theory of maximizing sensory information. *Biol. Cybern.* **68**, 23-29.
van Hateren, J. H. (1997). Processing of natural time series of intensities by the visual system of the blowfly. *Vision Res.* **37**, 3407-3416.
Wakakuwa, M., Stavenga, D. G. and Arikawa, K. (2007). Spectral organization of ommatidia in flower-visiting insects. *Photochem. Photobiol.* **83**, 27-34.
Wardill, T. J., List, O., Li, X., Dongre, S., McCulloch, M., Ting, C., O'Kane, C. J., Tang, S., Lee, C., Hardie, R. C. et al. (2012). Multiple spectral inputs improve motion discrimination in the *Drosophila* visual system. *Science* **336**, 925-931.
Weckström, M. and Laughlin, S. (2010). Extracellular potentials modify the transfer of information at photoreceptor output synapses in the blowfly compound eye. *J. Neurosci.* **30**, 9557-9566.
Weckström, M., Hardie, R. C. and Laughlin, S. B. (1991). Voltage-activated potassium channels in blowfly photoreceptors and their role in light adaptation. *J Physiol (Lond)* **440**, 635-657.
Yamaguchi, S., Wolf, R., Desplan, C. and Heisenberg, M. (2008). Motion vision is independent of color in *Drosophila*. *Proc. Natl. Acad. Sci. U.S.A.* **105**, 4910-4915.
Yang, E. C. and Osorio, D. (1996). Spectral responses and chromatic processing in the dragonfly lamina. *J Comp Physiol A* **178**, 543-550.
Zettler, F. and Järvilehto, M. (1971). Decrement-free conduction of graded potentials along the axon of a monopolar neuron. *Z Vergl Physiol* **75**, 402-421.